Technical Sciences
Academy of Romania
www.jesi.astr.ro

Journal of Engineering Sciences and Innovation
Volume 4, Issue 3 / 2019, pp. 301-312
http://doi.org/10.56958/jesi.2019.4.3.301
E. Electrical and Electronics Engineering

Received ***10 April 2019*** *Accepted* ***23 September 2019***
Received in revised from ***11 July 2019***

TP–Based model transformation and gain-scheduling control of electromagnetic actuated clutch systems

CLAUDIA-ADINA BOJAN-DRAGOS, ELENA-LORENA HEDREA, RADU-EMIL PRECUP*

AAI Department, Politehnica University Timisoara, Bd. V. Parvan 2, 300223 Timisoara, Romania

Abstract. This paper suggests two combinations of Tensor Product (TP)–based model transformation and gain-scheduling control leading to two efficient control system structures that are applied to the position control of nonlinear electromagnetic actuated clutch systems. One of the two combinations is included in a cascade control system structure that consists of a TP–based controller in the inner control loop and a gain-scheduling–based controller in the outer control loop. The proposed control system structures were tested on the nonlinear process model and validated by simulation results. A comparative analysis is given.

Keywords: cascade control system, electromagnetic actuated clutch systems, gain-scheduling control, mass position control, TP–based model transformation.

1. Introduction

This paper focuses on the development of two control structures (CSs) made of a combination of Tensor Product (TP)–based model transformation (TPBMT) and gain-scheduling control (GSC), which are applied to the position control of electromagnetic actuated clutch systems (EACSs). Our CSs are designed in the context of popular CS design approaches for EACS given in [1] – [5].
TPBMT is a numerical approach, which starts with Linear Parameter–Varying (LPV) dynamic models and derivates Linear Time-Invariant (LTI) systems as shown [6] – [9]. Representative applications of TPBMT are given in [10]–[15], and a combination of TPBMT and gain-scheduling control is presented in [16]. The combination with sliding mode control reported in [17] proves to be efficient by

* Correspondence address: radu.precup@aut.upt.ro

incorporating several theoretical and application results related to sliding mode control given in [18] – [21].
The main contribution of this paper is the design and validation of two CSs for the mass position control of EACS. In the first step a TP–based control structure (TP–CS) is designed for the position control of the EACS using the Parallel Distributed Compensation (PDC) technique, which is suitable for state feedback control, where a general nonlinear design approach is suggested and validated in on an inverted pendulum system application [22]. In the second step, a cascade control structure (GS-TP-CS) is designed for EACS with the TP–MT controller (TP–MT–C) in the inner control loop and the anti–windup Proportional–Integral–Derivative Gain–Scheduling controller (aw–PID–GS–C) in the outer control loop. The proposed CCSs are validated by simulation results. The comparison of these two types of CSs for EACS system, namely the TP–CS and the TP-GS-CS, is also given in this paper by means of a set of system responses and tracking error responses that can be easily compared.
The paper treats these topics: the mathematical model of the EACS is discussed in Section 2. The design of the two CCSs for EACS is briefly described in Section 3. The simulation results that illustrate the CCS performance and the comparative analysis are presented in Section 4. Section 5 highlights the conclusions.

2. Modelling of the controlled process

The process that is considered in this paper, modeled and next controlled, is an electromagnetic actuator clutch systems as part of a clutch system, illustrated in Fig. 1.

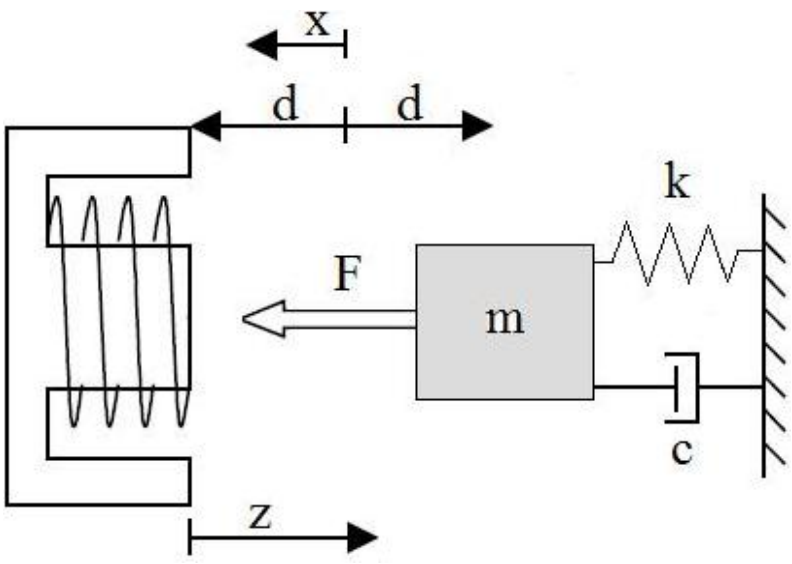

Fig. 1. Schematic structure of the magnetically actuated mass-spring-damper system.

In order to design the proposed CSs, the following nonlinear state-space model of the EACS is used in [23] – [25]:

$$\begin{aligned}
\dot{x}_1 &= x_2, \\
\dot{x}_2 &= -\frac{k}{m}x_1 - \frac{c}{m}x_2 + \frac{k_a x_3^2}{m(k_b + d - x_1)^2}, \\
\dot{x}_3 &= -\frac{R(k_b + d - x_1)}{2k_a}x_3 - \frac{1}{k_b + d - x_1}x_2 x_3 + \frac{k_b + d - x_1}{2k_a}u, \\
y &= 1000x_1,
\end{aligned} \tag{1}$$

where $u \in [0, 12]$ [V] is the control signal, $x_1 \in [0, 0.004]$ [m] is the mass position, x_2 [m/s] is mechanical subsystem's speed and $x_3 = \lambda$ [V·s] is the magnetic flux; y [m] is the measured mass position, m=1 [kg] is the mass, d=0.004 [m] is the distance between contact position and spring neutral position, R=1.2 [Ω] is the resistance, c=700 [N s/m] coefficient of the damper, k=37500 [N/m] is stiffness of the spring, k_a=0.5 is a constant k_b=0.375 is a constant, $i \in [0, 10]$ [A] is the current, and $F \in [0, 150]$ [N] is the external force.

3. Control structures design

In the following paragraphs the design of two CSs for the mass position control of EACS is detailed. The first CS is a TP–based control structure (TP–CS) designed for the position control of the EACS using the Parallel Distributed Compensation (PDC) technique. The second CS combines two CSs into a cascade control structure (TP-GS-CS): the TP–MT controller (TP–MT–C) in the inner control loop and the anti–windup Proportional–Integral–Derivative Gain–Scheduling controller (aw–PID–GS–C) in the outer control loop.

3.1. TP–based control structure design

Starting with the quasi–LPV (qLPV) model of EACS a TP–based control structure, namely TP–CS (Fig. 2), is designed, where u is the control signal, u_{TP} is the output of TP–based controller and r is the reference input.

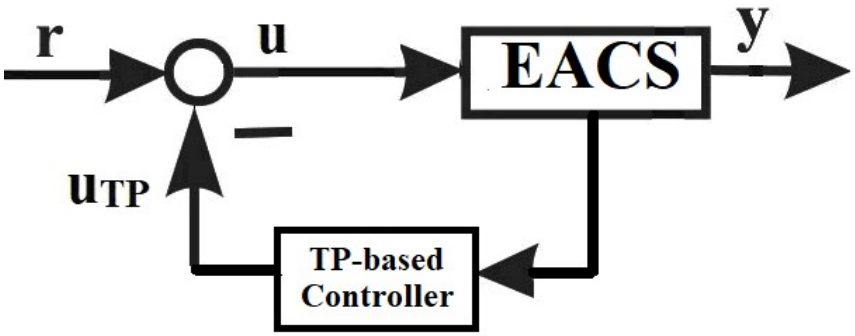

Fig. 2. Block diagram of TP–CS designed for EACS.

The qLPV model of EACS is

$$\begin{aligned} \dot{\mathbf{x}} &= \mathbf{A}(\mathbf{p})\mathbf{x} + \mathbf{b}(\mathbf{p})u, \\ y &= \mathbf{c}^T(\mathbf{p})\mathbf{x}, \end{aligned} \tag{2}$$

where $\mathbf{x} = \begin{bmatrix} x_1 & x_2 & x_3 \end{bmatrix}^T \in \Re^{3x1}$ is the process state vector, $\mathbf{p} = p_1 = x_1 \in \Re^{1x1}$ is the parameter vector (which contains the first state variable), y is the controlled output variable and the matrices $\mathbf{A}(\mathbf{p}), \mathbf{b}(\mathbf{p}), \mathbf{c}^T(\mathbf{p})$ are:

$$\mathbf{A}(\mathbf{p}) = \begin{bmatrix} 0 & 1 & 0 \\ a_{21}(\mathbf{p}) & a_{22} & a_{23}(\mathbf{p}) \\ a_{31}(\mathbf{p}) & a_{32}(\mathbf{p}) & a_{33}(\mathbf{p}) \end{bmatrix}, \mathbf{b}(\mathbf{p}) = \begin{bmatrix} 0 \\ 0 \\ k_b/(2k_a) \end{bmatrix}, \mathbf{c}^T(\mathbf{p}) = [1000 \quad 0 \quad 0], \tag{3}$$

$\mathbf{A}(\mathbf{p}) \in \Re^{3x3}$, $\mathbf{b}(\mathbf{p}) \in \Re^{3x1}$, $\mathbf{c}^T(\mathbf{p}) \in \Re^{1x3}$

where T indicates matrix transposition and the elements of the matrices are:

$$\begin{aligned} &a_{21} = -\frac{k}{m} + \frac{2k_a x_3^2}{m(k_b + d - \mathbf{p})^3}, a_{22} = -\frac{c}{m}, a_{23} = \frac{2k_a x_3}{m(k_b + d - \mathbf{p})^2}, \\ &a_{31} = \frac{Rx_3 - u}{2k_a} - \frac{x_2 x_3}{(k_b + d - \mathbf{p})^2}, a_{32} = -\frac{x_3}{k_b + d - \mathbf{p}}, a_{33} = -\frac{x_2}{k_b + d - \mathbf{p}} - \frac{R(k_b + d - \mathbf{p})}{2k_a}. \end{aligned} \tag{4}$$

Using the notation: $\mathbf{S}(\mathbf{p}) = [\mathbf{A}(\mathbf{p}) \quad \mathbf{b}(\mathbf{p})] \in \Re^{3\times 4}$, the qLPV model is obtained as follows:

$$\begin{aligned} \dot{\mathbf{x}} &= \mathbf{S}(\mathbf{p})[\mathbf{x}^T \quad u]^T, \\ y &= \mathbf{c}^T(\mathbf{p})\mathbf{x}, \end{aligned} \tag{5}$$

which aggregates a set of LTI models in terms of this process model:

$$\begin{aligned} \dot{\mathbf{x}} &= \mathbf{S}(\mathbf{p}(t)) \overset{N}{\underset{n=1}{\otimes}} \mathbf{w}_n(\mathbf{p}_n)[\mathbf{x}^T \quad u]^T = \sum_{i=1}^{I} w_{1,i}(p_1)\mathbf{S}_i[\mathbf{x}^T \quad u]^T, \\ y &= \mathbf{c}^T(\mathbf{p})\mathbf{x}, \end{aligned} \tag{6}$$

where $\mathbf{w}_n(\mathbf{p}_n)$ are the weighting functions, N is tensor's dimension, $\mathbf{S}$ is the $(N+2)$-dimensional coefficient tensor of the model given in (3) and I=3 is the number of singular values of the tensor $\mathbf{S}$ obtained after applying HOSVD to $\mathbf{S}$.

The LTI system matrices are $\mathbf{S}_i = [\mathbf{A}_i \quad \mathbf{b}_i]$, where the matrices $\mathbf{A}_i$ and $\mathbf{b}_i$ belong to the state-space system model

$$\begin{aligned} \dot{\mathbf{x}} &= \sum_{i=1}^{I} w_{1,i}(p_1)(\mathbf{A}_i\mathbf{x} + \mathbf{b}_i u), \\ y &= \mathbf{c}^T(\mathbf{p})\mathbf{x}, \end{aligned} \tag{7}$$

as a particular model of the general ones given in [22], and the matrix $\mathbf{c}^T(\mathbf{p})$ is constant in this application, i.e. $\mathbf{c}^T(\mathbf{p}) = \mathbf{c}^T$.

The asymptotic stabilization of the CS is the first control objective. It is achieved by the PDC technique, which determines one LTI state feedback gain matrix for each LTI vertex system of the convex TP model. The asymptotic stability of the closed–loop control system is equivalent to the existence of $\mathbf{X} = \mathbf{P}^{-1} > 0$ (where $\mathbf{P}$

is a positive definite matrix) and $\mathbf{M}_i$ that satisfy the following Linear Matrix Inequalities (LMIs) [8]:

$$\begin{aligned} &-\mathbf{X}\mathbf{A}_i^T - \mathbf{A}_i\mathbf{X} + \mathbf{M}_i^T\mathbf{X}_i^T + \mathbf{b}_i\mathbf{M}_i > 0, \\ &-\mathbf{X}\mathbf{A}_i^T - \mathbf{A}_i\mathbf{X} - \mathbf{X}\mathbf{A}_s^T - \mathbf{A}_s\mathbf{X} + \mathbf{M}_s^T\mathbf{b}_i^T \\ &+\mathbf{b}_i\mathbf{M}_s + \mathbf{M}_i^T\mathbf{B}_s^T + \mathbf{B}_s\mathbf{M}_i \geq 0,\ i = 1...3 \end{aligned} \tag{8}$$

in the Lyapunov-type formulation. However, Popov-type problem setting and expression of inequality-type stability conditions [26] can also be formulated and derived. The LTI state feedback gain matrices $\mathbf{F}_i$ are then computed as:

$$\mathbf{F}_i = \mathbf{M}_i\mathbf{X}^{-1}. \tag{9}$$

Finally, the application of PDC technique to EACS results in the following state feedback control law:

$$u = r - u_{TP} = r - \left[\sum_{i=1}^{3} w_{1,i}(p_1)\mathbf{F}_i\right]\mathbf{x}. \tag{10}$$

where u_{TP} is produced by the TP–based controller.

The second control objective is to constrain the control value. Let us assume that $\| \mathbf{x}(0) \|_2 \leq \phi$, where the initial state vector $\mathbf{x}(0)$ is unknown, but the upper bound ϕ is known. The constraint $|u| \leq \mu$ is enforced at all time moments if the following LMIs are satisfied [8]:

$$\phi^2\mathbf{I} \leq \mathbf{X}, \tag{11}$$

$$\begin{pmatrix} \mathbf{X} & \mathbf{M}_i^T \\ \mathbf{M}_i & \mu^2\mathbf{I} \end{pmatrix} \geq 0, \tag{12}$$

which guarantee that the second objective is achieved.

In this paper $\phi = 5.32 > 0$ and $\mu = 100$. The matrices $\mathbf{X}$ and $\mathbf{M}_i$ are computed using the YalmipR2015 solver. The solutions are next substituted in (9) leading to the following values of LTI state feedback gain matrices:

$$\begin{aligned} &\mathbf{F}_1 = \begin{bmatrix} 0.0093 & -0.0012 & -0.0003 \end{bmatrix}, \\ &\mathbf{F}_2 = \begin{bmatrix} -0.0005 & -0.0009 & 0.00017 \end{bmatrix}, \\ &\mathbf{F}_3 = \begin{bmatrix} -1.214 & -1.1749 & -1.36 \end{bmatrix}. \end{aligned} \tag{13}$$

3.2. The cascade control structure design

Due to the process nonlinearities, an aw–PID–GS–CS, Fig. 3, is employed in order to ensure the improvement of the CS performance such as the zero steady–state control error (or the tracking error), the alleviation of overshoot, and the bumpless switching between controllers [27].

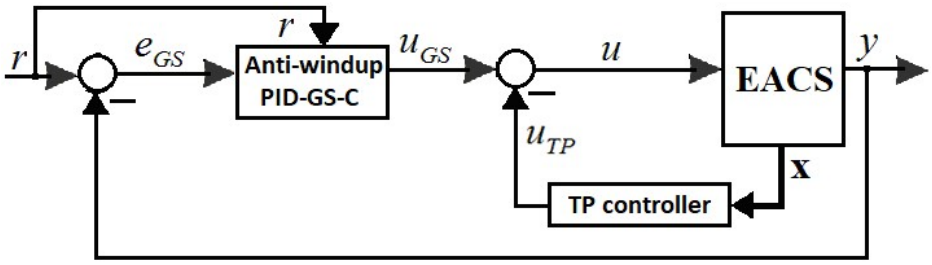

Fig. 3. Block diagram of CCS.

The design of this CS starts with a simple least-squares-based experimental approximation of the inner control loop (TP–CS) resulting in four third-order benchmark-type closed-loop transfer functions (t.f.s):

$$H_P^{(j)}(s) = \frac{k_P^{(j)}}{(1+T_1^{(j)}s)(1+T_2^{(j)}s)(1+T_3^{(j)}s)}, j = \overline{1,4}, \tag{14}$$

where $k_P^{(1)} = 0.34$, $k_P^{(2)} = 0.42$, $k_P^{(3)} = 0.61$, $k_P^{(4)} = 0.96$ are the inner control loop gains, $T_1^{(1)} = 0.065$, $T_1^{(2)} = 0.078$, $T_1^{(3)} = 0.085$, $T_1^{(4)} = 0.1$ are the large time constants, $T_2^{(1)} = 0.0156$, $T_2^{(2)} = 0.0162$, $T_2^{(3)} = 0.0165$, $T_2^{(4)} = 0.0168$, $T_3^{(1)} = T_3^{(2)} = T_3^{(3)} = T_3^{(4)} = 0.00166$ are the small time constants.

Using pole-zero cancellation four aw–PID–Cs were developed for the TP–CS with the t.f.s extended with a first–order lag filter:

$$H_C^{(j)}(s) = \frac{k_c^{(j)}}{s}(1+T_{c1}^{(j)}s)(1+T_{c2}^{(j)}s)\frac{1}{1+T_{fd}^{(j)}s}, j = \overline{1,4}, \tag{15}$$

with the tuning parameters $k_c^{(j)}$, $T_{c1}^{(j)}$, $T_{c2}^{(j)}$ and $T_{fd}^{(j)}$ obtained by the Modulus Optimum method, which is similar to the Symmetrical Optimum one and its extended version [28]:

$$k_c^{(j)} = \frac{1}{2 \cdot k_P^{(j)} \cdot T_3^{(j)}}, T_{c1}^{(j)} = T_1^{(j)}, T_{c2}^{(j)} = T_2^{(j)}, T_{fd}^{(j)} = 0.1 \cdot T_1^{(j)}, j = \overline{1,4}. \tag{16}$$

The output produced by the aw–PID–GS controller, u_{GS}, is expressed as:

$$u_{GS} = k_p(t)e_{GS}(t) + k_i(t)\int_0^t e_{GS}(\tau)d\tau + k_d(t)\dot{e}_{GS}(t), \tag{17}$$

with the tuning parameters, k_p, k_i and k_d obtained as follows [29]:

$$\begin{aligned} k_p(t) &= k_{p\max} - (k_{p\max} - k_{p\min})\exp[-(\alpha(t) \mid e(t) \mid)], \\ k_d(t) &= k_{d\max} - (k_{d\max} - k_{d\min})\exp[-(\alpha(t) \mid e(t) \mid)], \\ k_i(t) &= (1-\alpha(t))k_{i\max}. \end{aligned} \tag{18}$$

where the parameters $k_{p\max}$, $k_{p\min}$, $k_{d\max}$, $k_{d\min}$, $k_{i\max}$ and $k_{i\min}$ are computed using the tuning parameters of the aw–PID–Cs:

$$k_{p\max}=\max[k_c^{(j)}\cdot(T_{c1}^{(j)}+T_{c2}^{(j)})],\ k_{p\min}=\min[k_c^{(j)}\cdot(T_{c1}^{(j)}+T_{c2}^{(j)})],\ j=\overline{1,4}$$
$$k_{d\max}=\max(k_c^{(j)}\cdot T_{c1}^{(j)}\cdot T_{c2}^{(j)}),\quad k_{d\min}=\min(k_c^{(j)}\cdot T_{c1}^{(j)}\cdot T_{c2}^{(j)}),\quad j=\overline{1,4} \tag{19}$$
$$k_{i\max}=\max(k_c^{(j)}),\qquad k_{i\min}=\min(k_c^{(j)}),\qquad j=\overline{1,4}.$$

and the parameter $0\le\alpha(t)\le 1$ is chosen to ensure a smooth and continuous variation of the switching between aw–PID–Cs [29]:

$$\alpha(t)=\tanh(\eta\beta(t))=\frac{\exp(2\eta\beta(t))-1}{\exp(2\eta\beta(t))+1}, \tag{20}$$

The parameter η determines the rate at which $\alpha(t)$ changes between 0 and 1, and it is set to ensure a certain dynamics of the variation of $\alpha(t)$. The parameter $\beta(t)$ is set in terms of [30]:

$$\beta(t)=\begin{cases}1, & |e(t)|>\xi,\\ 0, & |e(t)|<\xi,\end{cases},\quad \xi=0.9\cdot r(t). \tag{21}$$

To design of aw–PID–GS–CS, the following conditions can be taken into account [29]: when $|e(t)|$ is large, $k_{p\max}$ and $k_{i\min}$ are activated to produce a large control signal and to reduce the undesirable oscillation and overshoot; the parameters, $k_{p\max}$ and $k_{i\min}$ are activated to obtain a small value of $|e(t)|$ and to reduce the high overshoot.

Finally, the control law u of the CCS is computed by combining output variable of TP–based controller, u_{TP} in (10), with the output variable of the aw–PID–GS controller, u_{GS}:

$$u=u_{GS}-u_{TP}=k_p(t)e_{GS}(t)+k_i(t)\int_0^t e_{GS}(\tau)d\tau+k_d(t)\dot{e}_{GS}(t)-\left[\sum_{i=1}^{3}w_{1,i}(p_1)\mathbf{F}_i\right]\mathbf{x}. \tag{22}$$

4. Simulation results

This section is dedicated to test the CSs discussed and designed in the previous sections, namely the TP–CS and the GS-TP-CS.

The following testing scenario was considered and performed: a staircase reference input acting for 10 s was applied to the nonlinear EACS and the corresponding outputs versus time for both the designed CSs are illustrated in Fig. 4. Zero initial conditions were used in the digital simulations that led to the simulation results presented in this paper.

The aw–PID–GS–C parameters $k_{p\max}=71.4$, $k_{p\min}=36$, $k_{d\max}=0.53$, $k_{d\min}=0.32$, $k_{i\max}=886$ and $k_{i\min}=314$ are determined using (21) and several experiments have been conducted such that to get the best values in the context of a compromise to tradeoff and overshoot.

In order to highlight the dynamic and steady-state performance of the two CSs designed in the previous sections, two performance indices were recorded and computed, namely the tracking error and the mean square error.

The tracking errors were computed as the difference between the reference input and the measured output of the TP–CS, y_{TP}, and as the difference between the reference input and the measured output of the GS–TP–CS, $y_{GS\text{-}TP}$.

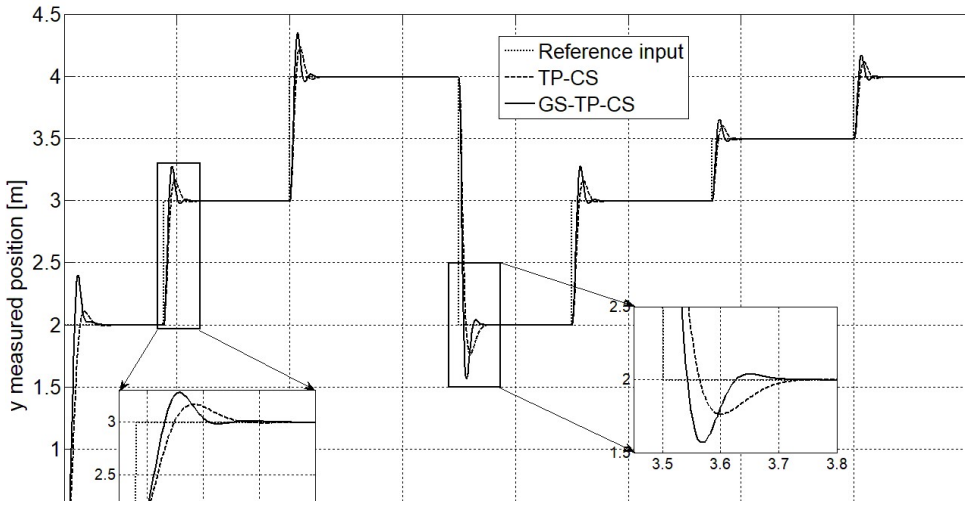

Fig. 4. Mass position vs time in the proposed CS with staircase reference signal.

The mean square error (MSE) was then computed for all the two CS as:

$$\mathrm{MSE}_{\mathrm{C}} = \frac{1}{N}\sum_{t_d=1}^{N}(r(t_d) - y_{\mathrm{C}}(t_d))^2, \tag{23}$$

where the subscript $\mathrm{C} \in \{\text{TP–CS, GS–TP–CS}\}$ indicates the designed CS, $r(t_d)$ is the reference at time moment $t_d = 1...N$, and N=3334 is the number of samples for staircase change inputs. The results are: $\mathrm{MSE}_{\text{TP-CS}} = 0.0876$ and $\mathrm{MSE}_{\text{GS-TP-CS}} = 0.0746$.

The simulation results prove that both the designed CSs ensure zero steady state control error and the reference is well tracked.

In case of GS–TP–CS the overshoot as a measure of the tracking error is bigger than in case of TP–CS, but the rise time and settling time are smaller. The smallest value of MSE was obtained in case of GS–TP–CS.

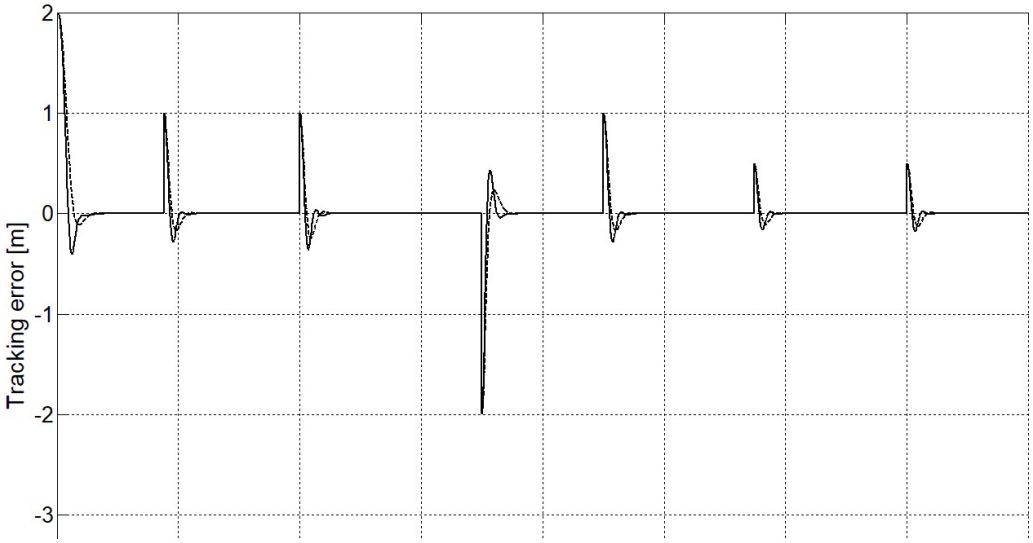

Fig. 5. Tracking error vs time in the proposed CS with staircase reference signal.

5. Conclusion

The paper presented the design and the validation of two CSs using a combination of Tensor Product (TP)–based model transformation and gain-scheduling control for mass position control of EACS, namely TP–CS and GS–TP–CS. The GS–TP–CS consists of an inner TP–based control loop and an outer gain-scheduling controller-based control loop.

The two CS structures were tested on a time horizon of 10 s applying a staircase type reference input. The simulation results prove that zero steady-state control error was ensured in case of both CSs. The best performance in terms of rise time, settling time and MSE is achieved in case of GS–TP–CS. However, a fair comparison should account for the complexity of the CS structures, and the cascade one is more complicated, hence it is normal to exhibit better over the non-cascade one. In addition, the number of tuning parameters and the simplicity of design procedure are important factors in the comparison.

Future research will be focused on the development of hybrid control techniques including TPBMT fuzzy control and gain-scheduling TPBMT nonlinear control using specific features of several nonlinear techniques outlined in [31]–[36] and various applications [37]–[42], aiming the further CS performance improvement.

Acknowledgment

This work was supported by the CNFIS-FDI-2019-0696 project of Politehnica University of Timisoara, Romania.

References

[1] B. Gao, H. Chen, Q. Liu, and H. Chu, Position control of electric clutch actuator using a triple-step nonlinear method, *IEEE Trans. Ind. Electron.*, **61**, no. 12, p. 6995–7003, Dec. 2014.
[2] J. J. Oh, S. B. Choi, and J. Kim, Driveline modeling and estimation of individual clutch torque during gear shifts for dual clutch transmission, *Mechatron.*, **24**, no. 5, p. 449–463, Aug. 2014.
[3] R. Losero, T.-M. Guerra, J. Lauber, and P. Maurel, Electro-mechanical clutch actuator control based on output switched Takagi-Sugeno controller, *IFAC-PapersOnLine*, **49**, no. 5, p. 85–90, Jun. 2016.
[4] R. Temporelli, P. Micheau, and M. Boisvert, Control of an electromechanical clutch actuator by a parallel adaptive feedforward and bang-bang controller: Simulation and experimental result, *IFAC-PapersOnLine*, **50**, no. 1, p. 4787–4793, Jul. 2017.
[5] A. Ranjan, S. Prasanth, F. Cherian, and P. Baskar, Design and control of electromagnetic clutch actuation system for automated manual transmission, *IOP Conf. Ser. Mat. Sci. Eng.*, **263**, p. 1–13, Oct. 2017.
[6] P. Baranyi, TP model transformation as a way to LMI based controller design, *IEEE Trans. Ind. Electron.*, **51**, no. 2, p. 387–400, Apr. 2004.
[7] Z. Petres, P. Baranyi, P. Korondi, and H. Hashimoto, Trajectory tracking by TP model transformation: Case study of a benchmark problem, *IEEE Trans. Ind. Electron.*, **54**, no. 3, p. 1654–1663, Jun. 2007.
[8] P. Baranyi, Y. Yam, and P. Varlaki, *TP Model Transformation in Polytopic Model-Based Control*. Boca Raton, FL: Taylor & Francis, 2013.
[9] R.-E. Precup, P. Angelov, B. S. J. Costa, and M. Sayed-Mouchaweh, An overview on fault diagnosis and nature-inspired optimal control of industrial process applications, *Comput. Ind.*, **74**, p. 75–94, Dec. 2015.
[10] P. Baranyi, TP model transformation as a manipulation tool for qLPV analysis and design, *Asian J. Control*, **17**, no. 2, p. 497–507, Mar. 2015.
[11] B. Takarics and P. Baranyi, TP type polytopic modelling of the Bergman minimal model of the diabetes mellitus, in *Proc. IEEE 17th Int. Conf. Intell. Eng. Syst.*, San Jose, Costa Rica, 2013, p. 73–78.
[12] P. Galambos, J. Kuti, P. Baranyi, G. Szögi, and I. J. Rudas, Tensor product based convex polytopic modeling of nonlinear insulin-glucose dynamics, in *Proc. 2015 IEEE Int. Conf. Syst. Man Cybern.,* Hong Kong, 2015, p. 2597–2602.
[13] J. Chen, R. F. Li, and C. Q. Cao, Convex polytopic modeling for flexible joints industrial robots using TP-model transformation, in *Proc. 2014 IEEE Int. Conf. Inf. Aut.*, Hailar, China, 2014, p. 1046–1050.
[14] E.-L. Hedrea, C.-A. Bojan-Dragos, R.-E. Precup, R.-C. Roman, E. M. Petriu, and C. Hedrea, Tensor product-based model transformation for position control of magnetic levitation systems, in *Proc. 26th Int. Symp. Ind. Electron.*, Edinburgh, UK, 2017, p. 1141–1146.
[15] J. Kuti and P. Galambos, Affine tensor product model transformation, *Complexity*, vol. 2018, p. 1–12, Jun. 2018.
[16] E.-L. Hedrea, C.-A. Bojan-Dragoş, R.-E. Precup, and E. M. Petriu, Comparative study of control structures for maglev systems, in *Proc. 2018 IEEE 18th Int. Conf. Power Electron. Motion Control*, Budapest, Hungary, 2018, p. 657–662.
[17] P. Korondi, Tensor product model transformation-based sliding surface design, *Acta Polyt. Hung.*, **3**, no. 4, p. 23–36, Dec. 2006.
[18] P. Korondi, H. Hashimoto, and V. Utkin, Discrete sliding mode control of two mass system, in *Proc. 1995 IEEE Int. Symp. Ind. Electron.*, Athens, Greece, 1995, p. 338–343.
[19] P. Korondi, H. Hashimoto, T. Gajdar, and Z. Suto, Optimal sliding mode design for motion control, in *Proc. 1996 IEEE Int. Symp. Ind. Electron.*, Warsaw, Poland, 1996, p. 277–282.
[20] P. Korondi and H. Hashimoto, Park vector based sliding mode control of UPS with unbalanced and nonlinear load, in: *Variable Structure Systems, Sliding Mode and Nonlinear Control*, K. D.

Young and Ü. Özgüner (Eds.), Springer-Verlag, London, Lecture Notes in Control and Information Sciences, **247**, p. 193–209, 1999.
[21] P. Korondi, K. D. Young, and H. Hashimoto, Sliding mode based disturbance observer for motion control, in *Proc. 37th IEEE Conf. Dec. Control*, Tampa, FL, USA, 1998, p. 1926–1927.
[22] C. Pozna and R.-E. Precup, An approach to the design of nonlinear state-space control systems, *Stud. Informat. Control*, **27**, no. 1, p. 5–14, Mar. 2018.
[23] S. Di Cairano, A. Bemporad, I. V. Kolmanovsky, and D. Hrovat, Model predictive control of magnetically actuated mass spring dampers for automotive applications, *Int. J. Control*, **80**, p. 1701–1716, Nov. 2007.
[24] R. H. Bishop, *Mechatronic Systems, Sensors, and Actuators: Fundamentals and Modeling*. Boca Raton, FL, USA: CRC Press, 2008.
[25] C.-A. Dragos, R.-E Precup, S. Preitl, E. M. Petriu, and A.-I. Stinean, Takagi-Sugeno fuzzy control solutions for mechatronic applications, *Int. J. Artif. Intell.*, **8**, no. S12, p. 45–65, Mar. 2012.
[26] R.-E. Precup and S. Preitl, Popov-type stability analysis method for fuzzy control systems, in *Proc. Fifth European Congress on Intelligent Technologies and Soft Computing*, Aachen, Germany, 1997, **2**, p. 1306–1310.
[27] C.-A. Dragos, S. Preitl., R.-E. Precup, E. M. Petriu, and A.-I. Stinean, Adaptive control solutions for the position control of electromagnetic actuated clutch systems, in *Proc. 2012 IEEE Intell. Veh. Symp.*, Alcala de Henares, Spain, 2012, p. 81–86.
[28] S. Preitl and R.-E. Precup, On the algorithmic design of a class of control systems based on providing the symmetry of open-loop Bode plots, *Scientific Bulletin of UPT, Transactions on Automatic Control and Computer Science*, **41** (55), no. 2, p. 47–55, Dec. 1996.
[29] A. Sedaghati, A PI controller based on gain-scheduling for synchronous generator, *Turkish J. Electr. Eng. Comput. Sci.*, **14**, no. 2, p. 241–251, Apr. 2006.
[30] C.-A. Bojan-Dragos, R.-E. Precup, S. Preitl, S. Hergane, E. G. Hughiet, and A.-I. Szedlak-Stinean, Proportional–integral gain–scheduling control of a magnetic levitation system, in *Proc. 20th Int. Conf. Syst. Theor. Control Comput.*, Sinaia, Romania, 2016, p. 1–6.
[31] R. Kelly, R. Haber, R. Haber-Guerra, and F. Reyes Cortes, Lyapunov stable control of robot manipulators: a fuzzy self–tuning procedure, *Intell. Autom. Soft Comput.*, **5**, no. 4, p. 313–326, Dec. 1999.
[32] R.-E. Precup and S. Preitl, Development of fuzzy controllers with non-homogeneous dynamics for integral-type plants, *Electr. Eng.*, **85**, no. 3, p. 155–168, Jul. 2003.
[33] E. H. Guechi, J. Lauber, M. Dambrine, G. Klančar, and S. Blažič, PDC control design for non-holonomic wheeled mobile robots with delayed outputs, *J. Intell. Robotic Syst.*, **60**, no. 3–4, p. 395–414, Dec. 2010.
[34] A. G. Khiabani and R. Babazadeh, Design of robust fractional-order lead–lag controller for uncertain systems, *IET Control Theor. Appl.*, **10**, no. 18, p. 2447–2455, Dec. 2016.
[35] R.-E. Precup and R.-C. David, *Nature-Inspired Optimization Algorithms for Fuzzy Controlled Servo Systems*. Oxford, UK: Butterworth-Heinemann, Elsevier, 2019.
[36] R. Andoga, L. Főző, R. Kovács, K. Beneda, T. Moravec, and M. Schreiner, Robust control of small turbojet engines, *Machines*, **7**, no. 3, p. 1–14, Jan. 2019.
[37] C. Pozna, R.-E. Precup, J. K. Tar, I. Škrjanc, and S. Preitl, New results in modelling derived from Bayesian filtering, *Knowl.-Based Syst.*, **23**, no. 2, p. 182–194, Mar. 2010.
[38] B. S. J. Costa, P. Angelov, and L. A. Guedes, Real-time fault detection using recursive density estimation, J. Control Autom. Electr. Syst., **25**, no. 4, p. 428–437, Dec. 2014.
[39] Á. Takács, L. Kovács, I. J. Rudas, R.-E. Precup, and T. Haidegger, Models for force control in telesurgical robot systems, *Acta Polyt. Hung.*, **12**, no. 8, p. 95–114, Dec. 2015.
[40] R. P. Alvarez Gil, Z. C. Johanyák, and T. Kovács, Surrogate model based optimization of traffic lights cycles and green period ratios using microscopic simulation and fuzzy rule interpolation, *Int. J. Artif. Intell.*, **16**, no. 1, p. 20–40, Mar. 2018.
[41] E. Ontiveros, P. Melin, and O. Castillo, High order α-planes integration: A new approach to computational cost reduction of general type–2 fuzzy systems, *Eng. Appl. Artif. Intell.*, **74**, p. 186–197, Sep. 2018.

[42] E. Osaba, R. Pierdicca, E. Malinverni, A. Khromova, F. Álvarez, and A. Bahillo, A smartphone–based system for outdoor data gathering using a wireless Beacon network and GPS data: From cyber spaces to senseable spaces, *ISPRS Int. J. Geo-Informat.*, **7**, no. 5, paper 190, Oct. 2018.